Journal of Solid State Chemistry 183 (2010) 2421–2425

Contents lists available at ScienceDirect

Journal of Solid State Chemistry

journal homepage: www.elsevier.com/locate/jssc

A one-pot synthetic approach to prepare palladium nanoparticles embedded hierarchically porous TiO_2 hollow spheres for hydrogen peroxide sensing

Lirong Kong, Xiaofeng Lu*, Xiujie Bian, Wanjin Zhang, Ce Wang*

Alan G. MacDiarmid Institute, Jilin University, Changchun 130012, PR China

ARTICLE INFO

Article history:
Received 18 June 2010
Received in revised form
4 August 2010
Accepted 5 August 2010
Available online 10 August 2010

Keywords:
Electrocatalytic
Mesoporous
Microporous
Nanocomposite

ABSTRACT

A simple one-step method to fabricate hierarchically porous TiO_2/Pd composite hollow spheres without any template was developed by using solvothermal treatment. Pd nanoparticles (2–5 nm) were well dispersed in the mesopores of the TiO_2 hollow spheres via in-situ reduction. In our experiment, polyvinylpyrrolidone played an important role in the synthetic process as the reducing agent and the connective material between TiO_2 and Pd nanoparticles. HF species generated from solvothermal reaction leaded to the formation of TiO_2 hollow spheres and Ostwald ripening was another main factor that affected the size and structure of the hollow spheres. The as-prepared TiO_2/Pd composite hollow spheres exhibited high electrocatalytic activity towards the reduction of H_2O_2. The sensitivity was about 226.72 $\mu A\ mM^{-1}\ cm^{-2}$ with a detection limit of 3.81 μM at a signal-to-noise ratio of 3. These results made the hierarchically porous TiO_2/Pd composite a promising platform for fabricating new nonenzymic biosensors.

1. Introduction

Accurate detection of H_2O_2 arouses great interest recently because H_2O_2, which is extremely toxic to cells, is not only an important analyte in many fields, including industry, clinical medicine and the environment, but also a byproduct of reactions catalyzed by many oxidase such as glucose oxidase and horseradish peroxidase [1–3]. Therefore, the rapid and accurate determination of H_2O_2 is of great importance in the field of environmental science and biochemistry. Among all the detective methods, using amperometric electrochemical sensor has been more and more investigated because of its low detection limit, less interference, low cost, fast response and being suitable for field analysis. Furthermore, as enzymes, such as glucose oxidase [4], cytochrome *c* [5], horseradish peroxidase [6–8], myoglobin [9] and hemoglobin [10,11], can accelerate the electron transfer between the electrodes and H_2O_2 due to their high catalytic activity, a great many scientists focused on preparing the enzyme-modified electrodes for H_2O_2 sensing because such electrodes can detect relatively low concentration of H_2O_2 with satisfactory sensitivity [12–20]. However, enzyme-modified electrodes still have some disadvantages which greatly limit their practical application, such as complicated immobilization procedure, critical operating situation, instability, high-cost of the enzymes, etc. Therefore, the development of simple, reliable and nontoxic nonenzymic electrodes for electroanalysis of H_2O_2 becomes necessary and pressing [21].

Recently, TiO_2 nanostructures, including nanotubes, nanorods and nanoparticles (NPs), have been more and more used as biosensors because of their large surface area, biocompatibility, stability and strong adsorptive ability on various electrode materials [22,23]. However, as pure TiO_2 nanostructures have little catalytic activity towards the reduction or oxidation of H_2O_2 and thus exhibit little sensitivity, the loading of catalytic materials such as various enzymes or noble metal NPs on TiO_2 nanostructures becomes necessary [12–21]. Among all the electrodes, nonenzymic TiO_2 based electrode showed lower sensitivity than those prepared with enzymes. Up to now, improving the sensitivity of such nonenzymic sensor is still a scientific crisis. Recently, some groups reported the preparation of hierarchically porous TiO_2 hollow spheres with high photocatalytic activity [24–26]. They attributed the high catalytic activity mainly to the novel structure because hierarchically porous TiO_2 hollow spheres possessed larger surface area than other TiO_2 materials and the mesoporous hollow structure could adsorb more analyte and prevent them from leaching. Based on these issues, if catalytic materials such as Pd NPs could be loaded in the mesopores of such hierarchically porous TiO_2 hollow spheres, the electrocatalytic activity towards the reduction of H_2O_2 may be greatly improved because of the abundant catalytic sites. However, the impregnation of Pd NPs into all the mesopores of TiO_2 hollow spheres is difficult to achieve by post-treatment because the pre-formed Pd

* Corresponding authors. Fax: +86 431 85168292.
E-mail addresses: xflu@jlu.edu.cn (X. Lu), cwang@jlu.edu.cn (C. Wang).

0022-4596/$ - see front matter © 2010 Elsevier Inc. All rights reserved.
doi:10.1016/j.jssc.2010.08.005

NPs on the surface of TiO_2 hollow spheres may block their way into the mesopores.

In this study, we have prepared Pd NPs embedded mesoporous TiO_2 hollow spheres in one step by using polyvinylpyrrolidone (PVP) as a connecting agent. In the final products, Pd NPs with a small diameter of 2–5 nm were evenly dispersed in the TiO_2 hollow spheres. Moreover, we investigated the influence of preparative conditions on the morphology of the final products and proposed the formation mechanism. At last, their electrocatalytic activity towards the reduction of H_2O_2 was investigated. In comparison to other nonenzymic and even enzymic electrodes [16–21], the TiO_2/Pd electrode presented high sensitivity, low potential, fast amperometric response and low detection limit to the detection of H_2O_2, which was promising for the development of nonenzymatic H_2O_2 sensor.

2. Experimental section

2.1. Materials

All the reagents were of analytical grade and used without further purification including TiF_4 (Alfa Aesar), $PdCl_2$ (Aldrich), $FeCl_3 \cdot 6H_2O$, PVP (K30), ethanol and concentrated hydrochloric acid (HCl). The water used in the experiments was distilled water.

2.2. Preparation of hierarchically porous TiO_2/Pd NPs hollow spheres

TiF_4 solution (0.017 M) was prepared by dissolving TiF_4 powder in 0.01 M HCl solution. 0.0125 M H_2PdCl_4 solution was prepared by dissolving $PdCl_2$ powder in 0.05 M HCl solution which was then heated for 5 min. The mixture of 34.5 mL ethanol containing 48.8 mg PVP, 6.25 mL 0.017 M TiF_4 solution and 5 mL 0.0125 M H_2PdCl_4 solution was ultrasonicated for 5 min and then stirred for another 30 min. 38 mL of the above mixture was poured into 40 mL Teflon-lined stainless-steel autoclave and then heated at 180 °C for 3 h. After the autoclaves cooled down naturally, the product was harvested by centrifugation and then washed with deionized water and ethanol before drying at 50 °C overnight.

2.3. Preparation of the modified electrodes

Before the modification, the basal glassy carbon electrode (GCE) was polished with alumina slurries polishing powder to a mirror finish. After each polishing, the electrode was ultrasonicated in sulfuric acid (1 M), ethanol and distilled water for 3 min, respectively, in order to remove any adhesive substances on the electrode surface. To modify the electrode, 5 μL TiO_2/Pd hollow nanospheres dispersion (5 mg/mL in water) was dropped on GCE surface and dried under ambient atmosphere.

2.4. Characterization

Transmission electron microscopy (TEM) experiments were performed on Hitachi 800 and 8100 electron microscopes (Tokyo, Japan) with an acceleration voltage of 200 kV. X-ray diffraction (XRD) patterns were obtained with a Siemens D5005 diffractometer using Cu$K\alpha$ radiation. Inductively coupled plasma atomic spectrum (ICP) was performed on Perkin Elmer OPTIMA 3300DV. Nitrogen adsorption–desorption isotherms were obtained on a TriStar 3000 nitrogen adsorption apparatus. All the samples were degassed at 200 °C for 10 h prior to Brunauer–Emmett–Teller (BET) measurements. The BET specific surface area was determined by a multipoint BET method. The desorption isotherm was used to determine the pore size distribution by using the Barret–Joyner–Halender (BJH) method. Pore volume was calculated according to the nitrogen adsorption–desorption isotherm. Electrochemical measurements were carried out at a CHI660c electrochemical workstation (Shanghai CH Instruments, China). These measurements were performed with a three-electrode configuration, consisting of the glassy carbon working electrode, an saturated calomel electrode (SCE) reference electrode and a platinum wire counter electrode, respectively.

3. Results and discussion

3.1. Formation mechanism and morphology of TiO_2/Pd composite hollow spheres

The process for fabricating TiO_2/Pd composite hollow spheres is shown in Scheme 1. In order to fully understand the formation mechanism of our composite hollow spheres, the morphologies of the products at different reaction time have been displayed. As the solvothermal process proceeded, TiF_4 quickly hydrolyzed to form small TiO_2 crystals which then aggregated together to form hollow spheres with an outer diameter of about 65–80 nm and an inner diameter of 20–40 nm when the reaction time was 0.5 h. The spheres were already hollow at the early period of reaction because with the hydrolysis of TiF_4, HF and TiO_2 gradually in situ formed with a molar ratio of 4:1 and the generated HF might enrich at the center of the spheres, creating a hollow interior [25]. Another possible reason is that the Ostwald ripening process happened at an early time of the reaction because the termination of the growth of the TiO_2 crystals was advanced. This is due to the fact that the absorbed PVP and Pd^{2+} limited the growth of TiO_2 nanocrystals which will be verified below using XRD data. Considering the fact that the hydrolysis of TiF_4 proceeded in an acidic environment, the HF etching may play a more important role in shaping the hollow spheres. At this period, Pd existed in the form of Pd^{2+} which was absorbed by PVP and then connected to the TiO_2 crystals. As a result, the product exhibited white color after being washed. When the reaction time was prolonged to 1.5 h, the TiO_2 spheres grew bigger because the inner TiO_2 crystals dissolved and outer TiO_2 crystals grew according to the Ostwald ripening process [26]. At this time, Pd^{2+} was reduced to Pd NPs by both PVP and the solvent under high temperature, so the color of the product turned to black. The diameter of the formed Pd NPs was so small because they were limited in the gap between the TiO_2 nanocrystals. For this reason, even the reaction time was further prolonged to 3 h or even 6 h, the diameter of Pd NPs almost did not change. However, the outer diameter and inner diameter of the TiO_2 hollow spheres gradually increased and achieved a maximum value of about 100–120 and 70–90 nm after reacting for 3 h. Further prolonging the reaction time would cause the hollow spheres to crack. Moreover, because of the van der Waals interaction between the cracked spheres, they would agglutinate

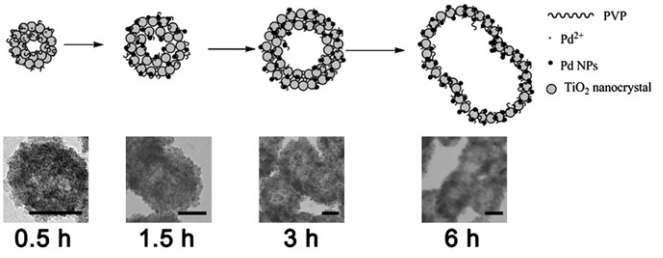

Scheme 1. Simplified schematic representations of the fabrication of TiO_2/Pd composite hollow spheres. Scale bar: 50 nm.

to form dimeric or multi-aggregated hollow spheres which can be seen in Scheme 1.

In order to further understand the affection of PVP, solvent and the added amounts of reactants to the morphology of the prepared samples, the morphologies of these products without PVP or using water as the solvent were investigated. We also observed their morphologies when the amounts of $PdCl_2$ or TiF_4 were changed. These results were all shown in Fig. 1. From the TEM image of pure TiO_2 shown in Fig. 1A, it could be found that they had similar diameters with TiO_2/Pd composite hollow spheres (Fig. 1B and C). The selected area electron diffraction (SAED) pattern of the hollow spheres (inset in Fig. 1A) revealed the polycrystalline nature of the TiO_2 hollow spheres. Fig. 1B showed a large area of the copper grid with more products. From it we could see that most of the products exhibited the morphology of well organized hollow spheres and small Pd NPs were evenly dispersed in TiO_2 matrix. In Fig. 1C, magnified TEM image of the composite hollow spheres showed that the diameters of the Pd NPs were in the range 2–5 nm. When PVP was not used in the reaction, fewer Pd NPs would attach on the surface of TiO_2 nanocrystals (Fig. 1D) because of the shortage of connective substance between Pd NPs and TiO_2 nanocrystals. As a result, isolated Pd NPs would aggregate into big block without supporting materials. Thus, PVP played an important role in forming well dispersed Pd NPs on TiO_2 nanocrystals. In addition to PVP, the type of solvent was another important factor which also greatly affected the morphology of the products. When the solvent of the reaction was changed from ethanol to water (Fig. 1E), the diameters of both TiO_2 crystals and Pd particles were more than 10 times larger than those synthesized in ethanol. The formation of bigger crystals was caused by the stronger hydrogen bond interaction in aqueous solution. In detail, when water was used as the solvent, the water molecules were adsorbed on the surface of TiO_2 and Pd particles. As a result, the strong hydrogen bond interaction between the water molecules would prompt these particles to get closer and then aggregate to form big agglomeration. Instead, when ethanol was used as the solvent, the hydrogen bond interaction was a lot weaker than that in water because of the lower density of the hydroxyl group. Then particles would not aggregate into big block, so small TiO_2 nanocrystals and Pd NPs could form and exist stably. Finally, the amount of the reactants were tuned to investigate the best condition for preparing TiO_2/Pd hollow spheres. As clearly shown in Fig. 1F, doubling the amount of TiF_4 would get bigger and thicker TiO_2 hollow spheres because TiO_2 nanocrystals formed and grew faster than before, thus more and bigger TiO_2 nanocrystals would easily aggregate into hollow sphere with bigger outer and inner diameters. Isolated TiO_2 nanocrystals also appeared in the final products. Comparatively, doubling the concentration of $PdCl_2$ would get more isolated Pd NPs (Fig. 1G). Contrarily, halving the amount of $PdCl_2$ could only get lower density of the Pd NPs loaded in the TiO_2 matrix (Fig. 1H). Using proper amounts of the reactants ($[TiF_4]=0.0023$ M, $[PdCl_2]=0.0014$ M, $[PVP]=1.06$ mg/mL), we could get composite spheres with best morphology in which the weight percentage of Pd is determined to be about 10.77% by ICP.

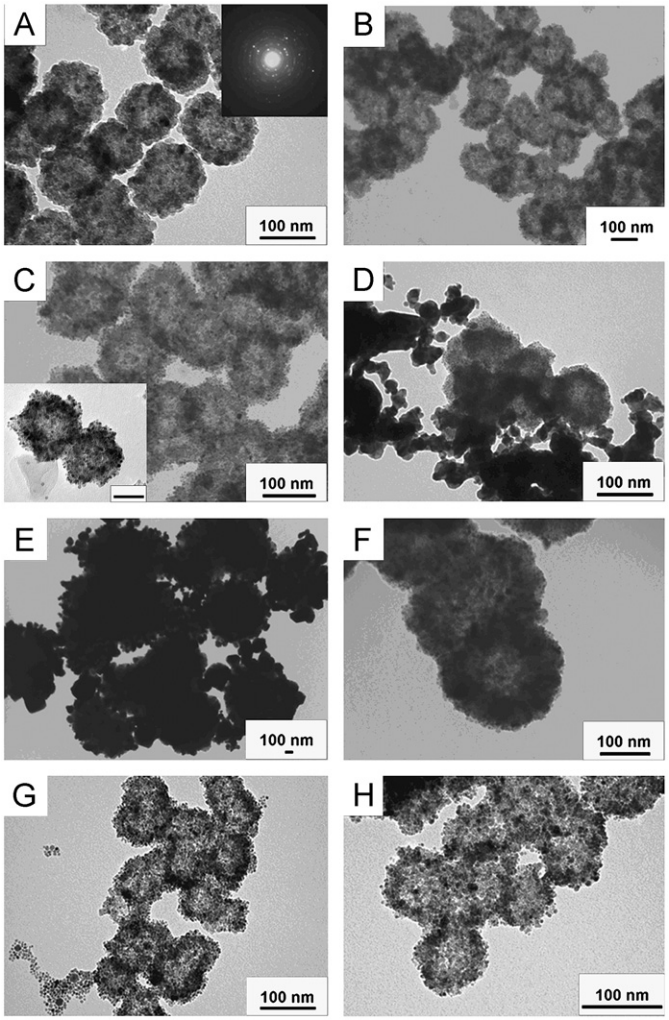

Fig. 1. TEM images of (A) pure TiO_2; (B) TiO_2/Pd; (C) magnified image of TiO_2/Pd (inset: two isolated TiO_2/Pd hollow spheres, the scale bar is 50 nm); (D) TiO_2/Pd (without PVP); (E) TiO_2/Pd (solvent: water); (F) TiO_2/Pd (using double amount of TiF_4); (G) TiO_2/Pd (using half amount of $PdCl_2$) and (H) TiO_2/Pd (using double amount of $PdCl_2$) composite hollow spheres. Inset in (A) shows the SAED pattern of individual TiO_2 hollow sphere.

3.2. Structure characterization

In order to further identify the crystal phase of the TiO_2 hollow spheres and Pd NPs, XRD was used to characterize their crystalline structure (Fig. 2). The as-synthesized products exhibited well-established peaks at $2\theta=25.22^\circ$, 37.78°, 47.82°, 53.82°, 54.86° and 62.5°, which could be ascribed to the (101), (004), (200), (105), (211) and (204) planes of anatase TiO_2 (JCPDS No. 21-1272) as reported by Zhou et al. [24]. The weak peak at $2\theta=22.68^\circ$ belonged to the Si background. Furthermore, in the XRD pattern of TiO_2/Pd composite hollow spheres, though the characteristic peaks of Pd NPs at 46.6° and 68.1°, which corresponded to (110)

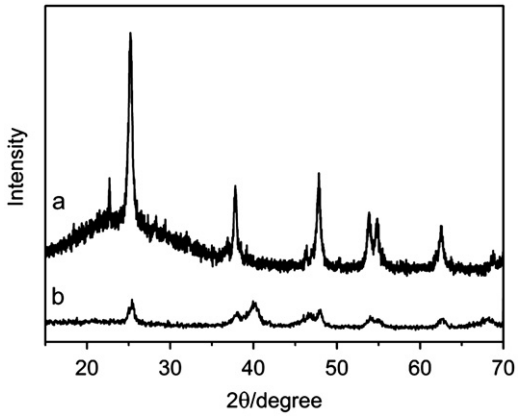

Fig. 2. XRD patterns of (a) pure TiO_2 hollow spheres and (b) TiO_2/Pd composite hollow spheres.

and (100) crystalline planes of Pd, were overlapped by the characteristic peaks of TiO_2 and could not be clearly observed, we could also observe the characteristic peaks of Pd NPs at $2\theta = 40.1^\circ$ which corresponded to (111) crystalline planes of Pd (JCPDS 5-0683). These results confirmed that the Pd^{2+} ions had been already reduced to Pd^0. According to Scherrer equation, the average crystal size of TiO_2 nanocrystal was 15.17 nm in pure TiO_2 hollow spheres and 10.1 nm in TiO_2/Pd nanocomposites. These data further verified the fact that absorbed PVP and Pd^{2+} limited the growth of TiO_2 crystals.

Nanoporous materials can always adsorb more analyte because of their larger surface area and this kind of adsorbing behavior is helpful in enhancing the sensitivity and shortening the response time towards the detection of H_2O_2. In order to confirm the hierarchically porous structure of the TiO_2/Pd composite spheres, nitrogen adsorption–desorption isotherm was performed and compared to that of the pure TiO_2 spheres. As shown in Fig. 3A, pure TiO_2 hollow spheres exhibited type IV with type H3 hysteresis loop while TiO_2/Pd exhibited type IV isotherm with type H4 hysteresis loop according to BDDT classification [27], indicating the presence of slit-like mesopores (2–50 nm) and macropores (>50 nm) in both of them [28,29].

Their pore size distributions further confirmed the results got from nitrogen adsorption–desorption isotherms. Two kinds of pores existed in TiO_2 hollow spheres: fine intra-aggregated pores formed between intra-agglomerated primary crystallites and large inter-aggregated pores produced by inter-aggregated secondary particles. The similar behavior was also observed in TiO_2/Pd composite hollow spheres. Such hierarchically porous structures in the as-prepared TiO_2/Pd composite hollow spheres could promote the rapid diffusion of analyte and improve their sensitivity to detect H_2O_2 during the electrocatalytic reaction. Fig. 3B indicated that TiO_2 hollow spheres contained small mesopores (peak pore ca. 6.02 nm), large mesopores and macropores (from 10 to 100 nm). However, the pore sizes in TiO_2/Pd composite hollow spheres were smaller than that in TiO_2 hollow spheres because Pd NPs took up part of the pore space between TiO_2 nanocrystals. From Fig. 3B, we could find that the pores in TiO_2/Pd composite hollow spheres small mesopores (peak pore below 3 nm and ca. 5.67 nm), large mesopores and macropores (from 10 to 90 nm). These results demonstrated the existence of hierarchically porous structures in the prepared samples on a multilength scale. The calculated BET surface areas of TiO_2 and TiO_2/Pd hollow spheres were 64.4 and 71.3 m^2/g while their pore volumes were 0.202 and 0.186 cm^3/g, respectively.

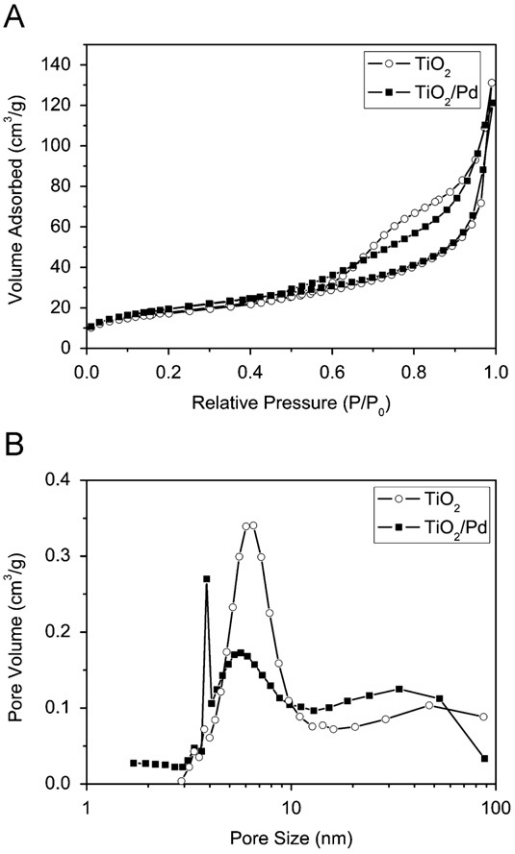

Fig. 3. (A) Nitrogen adsorption–desorption isotherm and (B) pore-size distribution of pure TiO_2 and TiO_2/Pd hollow spheres.

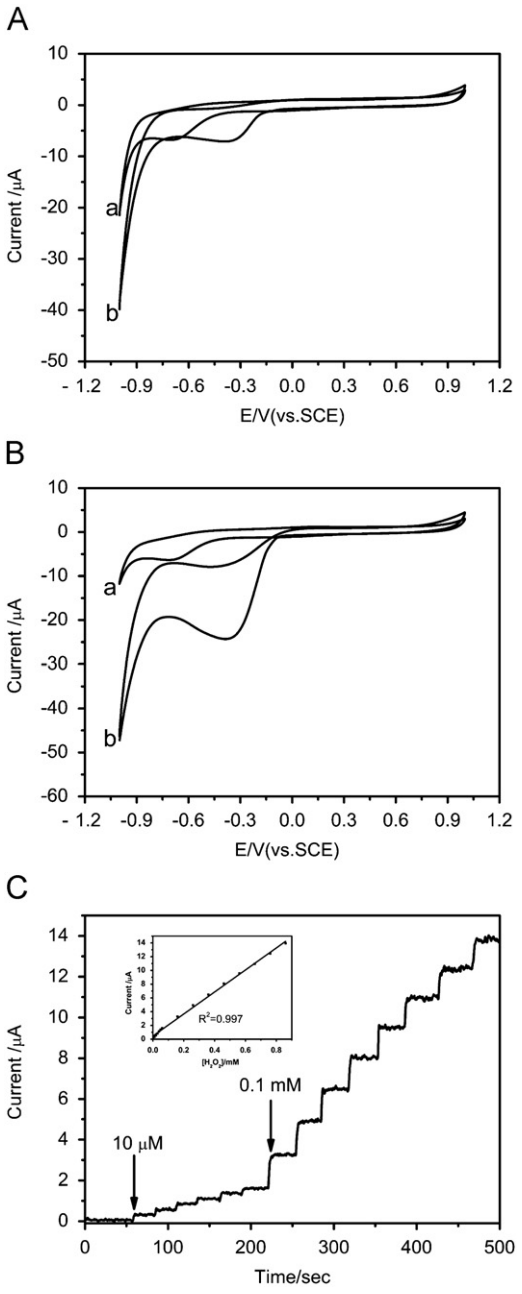

Fig. 4. CVs of (a) bare GC electrode and (b) TiO_2/Pd modified GC electrodes in (A) PBS (pH=7) and (B) PBS (pH=7) with 1 mM H_2O_2; (C) successive amperometric response of the TiO_2/Pd modified GC electrode to H_2O_2 in PBS (pH=7) at -0.2 V vs. SCE (inset: calibration curve for H_2O_2).

3.3. Electrochemical characterization

The sensing ability of the TiO_2/Pd hollow spheres modified GC electrode towards H_2O_2 was investigated and compared with bare GC electrode. The results are shown in Fig. 4. From Figs. 4A and B, it could be clearly observed that after the addition of 1 mM H_2O_2, the bare GC electrode displayed only a small current response to H_2O_2, indicating that bare electrode had little response to H_2O_2 because the reduction of H_2O_2 could hardly be achieved on it. However, when the electrode was modified with TiO_2/Pd hollow spheres, the current peak centered at about -0.3 V was greatly enhanced from -6.8 to -24.2 μA after the addition of 1 mM H_2O_2, indicating that the TiO_2/Pd modified electrode had high sensitivity towards H_2O_2. This was caused mainly by the catalytic activity of the Pd NPs loaded on TiO_2 hollow spheres.

In order to quantitatively determine the amount of H_2O_2 in practical sensor application, the amperometric responses of the modified electrode to successive injections of H_2O_2 at -0.2 V was recorded (Fig. 4C). According to the values of amperometric responses and the surface area of the working electrode which was 0.07065 cm^2, the sensitivity of the modified GC electrode could be calculated to be about 226.72 μA mM^{-1} cm^{-2}. Moreover, the sensor exhibited a linear dependence on H_2O_2 concentration ($R^2=0.997$) with a detection limit of 3.81 μM ($S/N=3$) in the range 0.01–0.86 mM. The sensitivity was higher than those on other TiO_2 based electrodes, including both nonenzymic and enzymic electrodes [16–21]. According to the experimental results, it was believed that the higher sensitivity was caused by the strong adsorptive ability and the high catalytic activity of the prepared hierarchically porous TiO_2/Pd hollow spheres. Their unique mesoporous structure offered more space for the adsorption of H_2O_2 and larger surface area as well as more catalytic sites towards the reduction of H_2O_2. During the electrocatalytic reaction, when analyte such as H_2O_2 was adsorbed to the electrocatalyst, the rate of the surface reaction which was the rate of electron transfer was increased. According to the above two reasons, a high response current was obtained. These results confirmed that the as-synthesized TiO_2/Pd hollow spheres possessed efficient electrocatalytic activity towards the reduction of H_2O_2, which had a potential application as a nonenzymic sensor for detecting H_2O_2.

4. Conclusions

In summary, a simple one-pot approach has been demonstrated to prepare TiO_2/Pd composite hollow spheres in which Pd NPs (2–5 nm) were well dispersed in the TiO_2 matrix and evenly attached on the surface of each TiO_2 nanocrystal. This method gives a new idea on how to prepare multifunctional nanocomposites with a well morphology and high activities. In our experiment, the modified electrode exhibit a high sensitivity (226.72 μA mM^{-1} cm^{-2}), a relatively low reduction potential (about -0.2 V), a fast response time (<3 s) and a relatively low detection limit of 3.81 μM ($S/N=3$) towards H_2O_2. It is expected that such hierarchically porous nanocrystalline TiO_2/Pd composite hollow spheres may also have great applications in photocatalysis, energy conversion device, separation and purification processes.

Acknowledgments

The financial support from the National 973 project (No. 2007CB936203) and the National Nature Science Foundation of China (Nos. 50973038 and 20904015) are greatly appreciated.

References

[1] O.S. Wolfbeis, A. Durkop, M. Wu, Z.H. Lin, Angew. Chem. Int. Ed. 41 (2002) 4495–4498.
[2] J.B. Jia, B.Q. Wang, A.G. Wu, G.J. Cheng, Z. Li, S.J. Dong, Anal. Chem. 74 (2002) 2217–2223.
[3] S.J. Guo, E.K. Wang, Anal. Chim. Acta 598 (2007) 181–192.
[4] C.X. Cai, J. Chen, Anal. Biochem. 332 (2004) 75–83.
[5] G.C. Zhao, Z.Z. Yin, L. Zhang, X.W. Wei, Elecreochem. Commun. 7 (2005) 256–260.
[6] V.S. Tripathi, V.B. Kandimalla, H.X. Ju, Biosens. Bioelectron. 21 (2006) 1529–1535.
[7] Y.D. Zhao, W.D. Zhang, H. Chen, Q.M. Luo, S.F.Y. Li, Sens. Actuators B 87 (2002) 168–172.
[8] Z.J. Cao, X.Q. Jiang, Q.J. Xie, S.Z. Yao, Biosens. Bioelectron. 24 (2008) 222–227.
[9] G.C. Zhao, L. Zhang, X.W. Wei, Anal. Biochem. 329 (2004) 160–161.
[10] H.L. Qi, C.X. Zhang, X.R. Li, Sens. Actuators B 114 (2006) 364–370.
[11] Y.D. Zhao, Y.H. Bi, W.D. Zhang, Q.M. Luo, Talanta 65 (2005) 489–494.
[12] Y. Astuti, E. Topoglidis, A.G. Cass, J.R. Durrant, Anal. Chim. Acta 648 (2009) 2–6.
[13] M.C. Liu, G.H. Zhao, K.J. Zhao, X.L. Tong, Y.T. Tang, Electrochem. Commun. 11 (2009) 1397–1400.
[14] G.D. Jiang, H.Q. Tang, L.H. Zhu, J.D. Zhang, B. Lu, Sens. Actuators B 138 (2009) 607–612.
[15] L. Zhang, D.B. Tian, J.J. Zhu, Bioelectrochemistry 74 (2008) 157–163.
[16] S.A. Kumar, P.H. Lo, S.M. Chen, Nanotechnology 19 (2008) 255501 (7pp).
[17] A.W. Zhu, Y.P. Luo, Y. Tian, Anal. Chem. 81 (2009) 7243–7247.
[18] G.H. Zhao, Y.Z. Lei, Y.G. Zhang, H.X. Li, M.C. Liu, J. Phys. Chem. C 112 (2008) 14786–14795.
[19] P.H. Lo, S.A. Kumar, S.M. Chen, Colloids Surf. B 66 (2008) 266–273.
[20] Y.T. Shi, R. Yuan, Y.Q. Chai, X.L. He, Electrochim. Acta 52 (2007) 3518–3524.
[21] L.C. Jiang, W.D. Zhang, Electroanalysis 21 (2009) 988–993.
[22] E. Topoglidis, B.M. Discher, C.C. Moser, P.L. Dutton, J.R. Durrant, ChemBioChem 4 (2003) 1332–1339.
[23] K.J. McKenziea, F. Markena, M. Opallo, Bioelectrochemistry 66 (2005) 41–47.
[24] J.K. Zhou, L. Lv, J.Q. Yu, H.L. Li, P.Z. Guo, H. Sun, X.S. Zhao, J. Phys. Chem. C 112 (2008) 5316–5321.
[25] J.G. Yu, W. Liu, H.G. Yu, Cryst. Growth Des. 8 (2008) 930–934.
[26] H.G. Yang, H.C. Zeng, J. Phys. Chem. B 108 (2004) 3492–3495.
[27] K.S.W. Sing, D.H. Everett, R.A.W. Haul, L. Moscou, R.A. Pierotti, J. Rouquerol, T. Siemieniewska, Pure Appl. Chem. 57 (1985) 603–619.
[28] D.V. Bavykin, V.N. Parmon, A.A. Lapkin, F.C. Walsh, J. Mater. Chem. 14 (2004) 3370–3377.
[29] H.G. Yu, J.G. Yu, B. Cheng, J. Lin, J. Hazard. Mater. 147 (2007) 581–587.